Check for updates

JGR Space Physics

RESEARCH ARTICLE
10.1029/2022JA030565

Transient Response of Polar-Cusp Ionosphere to an Interplanetary Shock

Jianjun Liu[1,2], Shibaji Chakraborty[3], Xiangcai Chen[1,2], Zhiwei Wang[1], Fang He[1], Zejun Hu[1,2], Erxiao Liu[4], Amarjargal Bat-Erdene[5], Desheng Han[6], J. Michael Ruohoniemi[3], Joseph B. H. Baker[3], Huigen Yang[1], Qiugang Zong[1,7], and Hongqiao Hu[1,2]

[1]MNR Key Laboratory for Polar Science, Polar Research Institute of China, Shanghai, China, [2]Antarctic Zhongshan National Field Observation and Research Station for Snow and Ice, Space Special Environment and Disasters, Polar Research Institute of China, Shanghai, China, [3]Bradley Department of Electrical and Computer Engineering, Virginia Tech, Blacksburg, VA, USA, [4]College of Communication Engineering, Hangzhou Dianzi University, Hangzhou, China, [5]Department of Geomagnetic, Institute Astronomy and Geophysics, Mongolian Academy of Science, Ulaanbaatar, Mongolia, [6]State Key Laboratory of Marine Geology, School of Ocean and Earth Science, Tongji University, Shanghai, China, [7]Institute of Space Physics and Applied Technology, Peking University, Beijing, China

Key Points:

- Ionosonde ZHO detected enhanced *E* region ionization and vertical plasma motion following the arrival of an interplanetary shock
- Evidence suggests that the strong *E* layers are the result of sudden impulse (SI)-driven E-field drift-convergence and particle precipitation
- IP shock-triggered SI alters the dusk-to-dawn electric field that drives a brief downward plasma motion at the dayside polar ionosphere

Correspondence to:

S. Chakraborty and Z. Hu,
shibaji7@vt.edu;
huzejun@pric.org.cn

Citation:

Liu, J., Chakraborty, S., Chen, X., Wang, Z., He, F., Hu, Z., et al. (2023). Transient response of polar-cusp ionosphere to an interplanetary shock. *Journal of Geophysical Research: Space Physics*, *128*, e2022JA030565. https://doi.org/10.1029/2022JA030565

Received 20 APR 2022
Accepted 1 MAR 2023

Author Contributions:

Conceptualization: Jianjun Liu
Data curation: Fang He
Formal analysis: Jianjun Liu
Investigation: Jianjun Liu
Methodology: Shibaji Chakraborty
Resources: Jianjun Liu
Software: Xiangcai Chen, Fang He
Supervision: Qiugang Zong
Validation: Xiangcai Chen
Visualization: Shibaji Chakraborty
Writing – original draft: Jianjun Liu
Writing – review & editing: Shibaji Chakraborty, Huigen Yang

©2023. The Authors.
This is an open access article under the terms of the Creative Commons Attribution License, which permits use, distribution and reproduction in any medium, provided the original work is properly cited.

Abstract Interplanetary (IP) shock-driven sudden compression of the Earth's magnetosphere produces electromagnetic disturbances in the polar ionosphere. Several studies have examined the effects of IP shock on magnetosphere-ionosphere coupling systems using all-sky cameras and radars. In this study, we examine responses and drivers of the polar ionosphere following an IP shock compression on 16 June 2012. We observe the vertical drift and concurrent horizontal motion of the plasma. Observations from digisonde located at Antarctic Zhongshan station (ZHO) showed an ionospheric thick *E* region ionization and associated vertical downward plasma motion at *F* region. In addition, horizontal ionospheric convection reversals were observed on the Super Dual Auroral Radar Network ZHO and McMurdo radar observations. Findings suggest that the transient convective reversal breaks the original shear equilibrium, it is expected that the IP shock-induced electric field triggers an enhanced velocity shear mapping to the *E* region. The horizontal motion of the plasma was attributed to only the dusk-to-dawn electric field that existed during the preliminary phase of sudden impulse. We also found that ionospheric convection reversals were driven by a downward field-aligned current. The results of these observations reveal, for the first time, the immediate and direct cusp ionosphere response to the IP shock, which is critical for understanding the global response of the magnetosphere following an abrupt change in Interplanetory Magnetic Field (IMF) and solar wind conditions.

Plain Language Summary On 16 June 2012, an interplanetary (IP) shock hit near-Earth space (geospace), resulting in enhanced plasma convection, auroral intensifications, and altering electric current systems in the high- and polar-latitude ionosphere. We present a case study characterizing the effect of IP shock-driven sudden impulse (SI) impact on geospace systems that changes vertical drift and horizontal convection observed by digital ionosonde and Super Dual Auroral Radar Network high-frequency radars. We found an SI-driven immediate vertical downward plasma motion, the sudden appearance of sporadic E-layer, and an ionospheric convection reversal following the IP shock. We discuss the possible impact of SI on magnetospheric-ionospheric coupling systems and possible driving mechanisms that are attributed to the observations reported in the study.

1. Introduction

Geomagnetic field and plasma convection on Earth are strongly affected by interplanetary (IP) shocks and solar wind dynamic pressure pulses [P_{dyn}] (e.g., Boudouridis et al., 2007; Yue et al., 2010). After the IP shock hits the magnetosphere, the magnetopause moves inward, toward the Earth and the eastward magnetopause current intensifies rapidly as a result of this prompt compression (Araki, 1994). In consequence, the horizontal component of the geomagnetic field in low and mid-latitudes typically responds with an abrupt increase due to an enhanced eastward magnetopause current. This sudden increase in the horizontal component of the geomagnetic field on the dayside is referred to as an sudden impulse (SI) event with a precise onset time (Araki, 1994). In comparison with their clear stepwise signatures in the lower latitude regions, SI-associated geomagnetic disturbances at

21699402, 2023, 3, Downloaded from https://agupubs.onlinelibrary.wiley.com/doi/10.1029/2022JA030565, Wiley Online Library on [11/07/2024]. See the Terms and Conditions (https://onlinelibrary.wiley.com/terms-and-conditions) on Wiley Online Library for rules of use; OA articles are governed by the applicable Creative Commons License

the high latitudes are predominantly caused by more complex physical phenomena. Depending on the ground magnetic bipolar signature at auroral latitudes, the geomagnetic perturbation at high latitudes can be decomposed into a preliminary impulse (PI) and subsequent main impulse (Araki, 1994).

Early experimental results using Very Low Frequency (VLF) receivers and high-frequency (HF) Doppler sounders in the high-latitude region revealed that SI-associated phase anomalies are observed during the night with relatively lower solar and geomagnetic activities (Kikuchi et al., 1986). In addition, the IP shock compression enhances the magnetic reconnection process at the dayside magnetopause and nightside magnetotail (Boudouridis et al., 2004, 2007, 2008; Zhou et al., 2003). As a result of an external force, plasma bound to magnetic field lines circulates with reconnected field lines in the magnetosphere, which speeds up the transmission of energy (Ilie et al., 2010). Simulation result also reveals an intensification of high-latitude horizontal $\vec{E} \times \vec{B}$ plasma drift velocity following an IP shock compression (Slinker et al., 1999).

The IP shock interacting with geospace affects the ionosphere via a highly coupled magnetosphere-ionosphere system. The ground-based Global Positioning System (GPS) observations suggest that the entire equatorial and mid-latitude dayside ionosphere can be uplifted by significantly increasing the electron content (and densities) at altitudes greater than 430 km (Tsurutani et al., 2004). Using the ground-based digisonde from the global ionospheric radio observatory, Zong et al. (2010) examined two IP shock-associated ionospheric response events. The study reported that the ionospheric plasma in the equatorial regions moves up and downward under the southward and northward IMF conditions, respectively. In middle and high-latitudes, total electron content (TEC) estimated from wide distributed Global Navigation Satellite System (GNSS) receivers showed an enhancement in plasma along the dawn and dusk sectors of the auroral oval (Jin et al., 2016). Coordinated observations from the global GNSS receiver network reveal a prompt and intense ionospheric TEC in response to the IP shock. In addition, GPS receiver data at the Canadian High Arctic Ionospheric Network shows an enhancement in TEC observations following compression of the magnetosphere in response to a sudden increase in solar wind dynamic pressure (Jayachandran et al., 2011). A study by Jayachandran et al. (2011) suggested that PI shock-driven TEC enhancement is attributed to the *F*-region increased electron density due to particle precipitation. TEC provides quantitative estimates of the ionospheric volume electron content associated with the IP shock impingement, it is unable to depict the ionospheric electrodynamics and convection. In this study, we aim to show the transient response of ionospheric electrodynamics following an IP shock near the polar cusp and auroral ionosphere. In addition, we also present the vertical and horizontal plasma convection in response to an external IP shock and infer their drivers. The scientific merit of the study lies in the fact that it provides insight into the magnetosphere-ionosphere system and its response to external perturbed solar wind plasma forcing during an increase in P_{dyn}.

In this study, we primarily examine the effects of the IP shock on the polar cusp ionosphere. Specifically, we observe the three-dimensional motion of the polar ionosphere and its spatiotemporal evolution in response to the IP shock event using Super Dual Auroral Radar Network (SuperDARN) radars and a digisonde located at the ZHO station in Antarctica. The location of ZHO digisonde makes it optimal to observe the dynamics of the cusp ionosphere near magnetic noon. Convection maps and ionograms obtained from the SuperDARN radars and the ionosonde, respectively, are analyzed to understand the dynamics of polar ionospheric plasma motion following the IP shock and their drivers.

2. Instrumentation and Data Set

Data from the WIND satellite, located upstream of the dayside magnetopause (Lepping et al., 1995), provides information about the solar wind plasma conditions. Using the geomagnetic SYM-H index, we can describe the associated global geomagnetic variations caused by external solar wind forcing.

The ionospheric drift motion over ZHO was obtained from digital ionosonde (digisonde) observations. Figure 1 presents the location of the ZHO station (geographic coordinate: 69.4°S, 76.4°E). The digisonde at ZHO is a vertical radar that uses HF (3–30 MHz) radio waves to remote sense the ionospheric plasma density structures, irregularities (Reinisch et al., 2009), and vertical apparent motion of the plasma. ZHO digisonde uses the near-vertical sounding technique to measure backscatter echoes from the ionospheric plasma density structures. In addition, a digisonde measures the Doppler frequency shifts to measure the line-of-sight (LoS) Doppler velocity for individual echoes. With the help of the elevation look angle of the system, virtual height models, and least square fitting, we can decompose the observed LoS Doppler velocity to its vertical and horizontal components

21699402, 2023, 3, Downloaded from https://agupubs.onlinelibrary.wiley.com/doi/10.1029/2022JA030565, Wiley Online Library on [11/07/2024]. See the Terms and Conditions (https://onlinelibrary.wiley.com/terms-and-conditions) on Wiley Online Library for rules of use; OA articles are governed by the applicable Creative Commons License

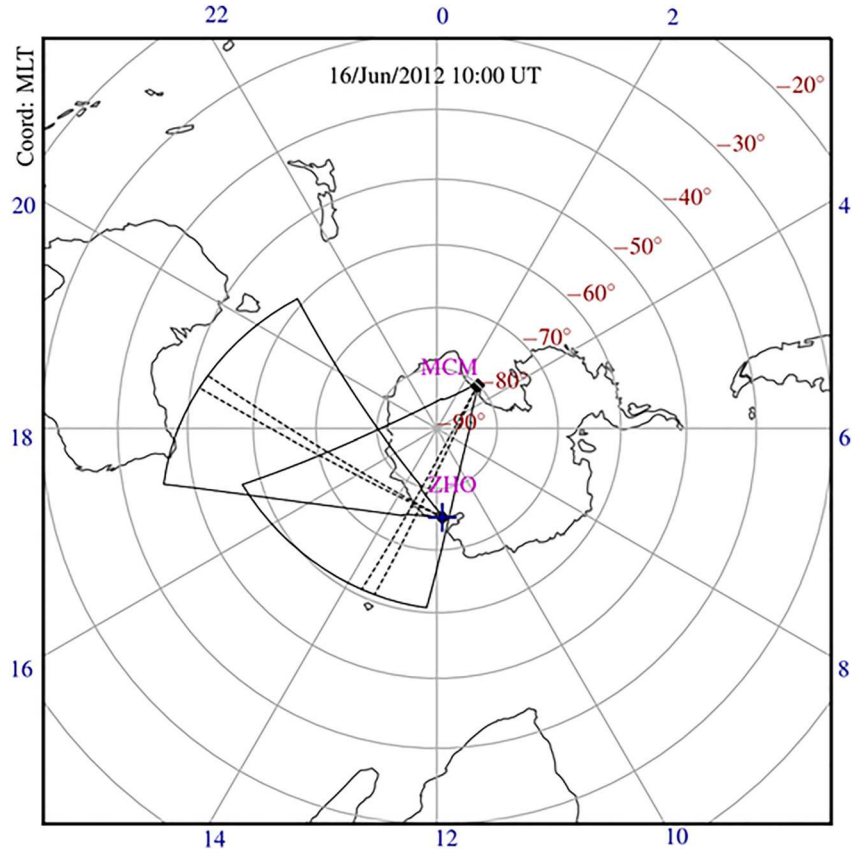

Figure 1. The field-of-view of the Super Dual Auroral Radar Network radars is located at the ZHO and McMurdo (MCM) stations in the southern hemisphere. Concentric circles indicate magnetic latitude (in intervals of 10°), and radial lines indicate magnetic local time (at intervals of 3 hr). The beams 7 and 4 of the ZHO radar and the MCM radar are plotted, respectively, to illustrate the spatial extent of radar look direction near noon. The blue plus (+) sign on the ZHO station represents the digisonde.

(e.g., Chen et al., 2022). ZHO digisonde currently operates with the following parameter set frequency range of 0.5–9.5 MHz and has height, Doppler, and temporal resolutions of 2.5 km, 0.1302 Hz, and 5 min (Liu et al., 1997). A full scan of vertical sounding can be displayed as ionograms and skymaps. Assuming the ionosphere height of the radio wave from the digisonde is 300 km, the Skymap area scanned by the digisonde extends from ∼73.5° to ∼76.5° magnetic latitude (MLAT) (Liu & Zhu, 1999). The ionogram and skymap provide insight into the localized variations in ionospheric plasma structures. ZHO is situated right beneath of the auroral oval on the dayside sector, and close to the poleward boundary of the oval or in polar cap region on the nightside sector, as illustrated in Figure 1. Therefore, digisonde observations allow us to study the dynamics of the cusp ionosphere in response to changes in the solar wind.

To characterize ionospheric horizontal convection in response to the IP shock impingement, we analyzed the fitacf-level LoS observations from SuperDARN ZHO and McMurdo (MCM) HF radars. In addition, we have used map-level SuperDARN convection summary maps, generated using observations from multiple radars, to examine the ionospheric plasma dynamics. SuperDARN is an international collaboration of HF radars and operates between 8 and 20 MHz, distributed mainly from mid-to high-latitude to probe the upper atmosphere and ionosphere (Chisham et al., 2007; Greenwald et al., 1995; Nishitani et al., 2019). SuperDARN ZHO radar consists of two radar channels, which can transmit and receive signals independently but share the same hardware system (Hu et al., 2013; Liu et al., 2012). The Fields-of-View (FoV) of the SuperDARN radar located at MCM station is oriented such that the geomagnetic pole lies in the middle of the radar FoV (Bristow et al., 2011). FoVs of both SuperDARN HF radars is presented in Figure 1. We can see that the orientation of the MCM radar provides a substantial overlap with the FoV of the ZHO radar. The dashed line in the FoV of ZHO and MCM radars indicates beam 7 and beam 4 of the radars, respectively. SuperDARN backscattered Doppler echoes, which are primarily

backscatter from field-aligned plasma irregularities (Lester et al., 2004), are used to derive backscatter power, LoS Doppler velocity, and spectral width parameters. In particular, such conjunctive observations by these three remote sensing instruments obtain the transient ionosphere response to the external solar wind forcing. Besides these two radars, we have used data from five other SuperDARN radars to build the summary convection maps to analyze switching in horizontal convection velocity following the SI impingement.

In addition, the relative ionospheric opacity meter, or riometer, offers a routine ground-based method for monitoring moderately energetic particle precipitation (Little & Leinbach, 1959). We also use the ionospheric absorption measurement from a riometer at Yellow River station in Northern Hemisphere Svalbard, which is magnetically conjugate to the ZHO. To verify the geomagnetic response to the approaching IP shock prompt compression to the magnetosphere, observations by five fluxgate magnetometers distributed from high latitude to low latitude were examined.

3. Observational Results

This section discusses the observations obtained from the digisonde and SuperDARN radars on 16 June 2012. As a first step, we present IMF and solar wind conditions from the WIND satellite as well as information about their effects on the geospace from ground-based magnetometers located from the equator to southern high latitudes. Additionally, we present the ionospheric vertical plasma motion as observed by the ZHO digisonde, as well as a change in the horizontal LoS Doppler velocity as observed by the SuperDARN ZHO and MCM radars during the PI of the SI. Finally, we present the global scale plasma convection summary maps to demonstrate the global scale ionospheric plasma motion in response to the IP shock.

3.1. The IP Shock and the Associated Geomagnetic Disturbance

IMF and solar wind plasma parameters between 08:00 and 10:00 UT, measured by the WIND satellite, located between the Sun and Earth at ($227R_E$, $-99R_E$, $20R_E$) in GSM coordinate system, are presented in Figure 2a. The temporal resolutions of the IMF and solar wind plasma data are 16-s and 64-s, respectively. The top three panels in Figure 2a display the total IMF B_t, B_x (in black) and B_y (in red), and B_z components in the GSM coordinate, respectively. Before 09:02 UT, the IMF was relatively stable, which resulted in a relatively stable interplanetary (IP) environment. IMF B_x remains steady, weak, and anti-sunward for the entire period before 09:02 UT. IMF B_y indicates a sudden and rapid increase and then becomes positive at 09:02 UT and afterward. In addition, IMF B_z shows a relatively small increase in magnitude following a sudden fluctuation around zero. These sharp fluctuations in IMF B_y and B_z components resulted in a sudden increase of B_t, as shown in the top panel of Figure 2a.

In Figure 2a, the bottom three panels present parameters of the solar wind plasma, including number density N_{sw}, solar wind velocity V_{sw}, and dynamic pressure P_{dyn}, for the same time interval as the IMF parameters. In addition, the solar wind plasma parameters were also stable before 09:02 UT with a relatively low N_{sw} (4/cc) and a nearly constant plasma speed of 300 km/s. The WIND satellite, however, recorded a noteworthy change in N_{sw} from 4/cc to 11/cc and in V_{sw} from 300 to 400 km/s at ∼09:02 UT. As a result of the variations in these two plasma parameters, solar wind P_{dyn} increased immediately from 0.5 to 3 nPa, as shown by the vertical red dashed line in Figure 2a. These are characteristic features of a fast-forward IP shock approaching the geospace.

In Figure 2b, the six panels from top to bottom depict the horizontal components of the geomagnetic field recorded by five different ground-based magnetometers and the SYM-H index between the time interval of 09:30–10:30 UT, that is, during the IP shock passage. Magnetometers are listed according to their magnetic latitude in descending order. The associated MLAT and MLT (magnetic local time) information for each magnetometer observatory is provided in panels of Figure 2b. Note that the geomagnetic field data has a one-minute temporal resolution. The SYM-H index in the bottom panel shows that the approaching IP shock arrived at the dayside magnetopause at ∼09:56 UT, which indicates that the IP shock propagated almost 54 min to reach near Earth's space from the location of the WIND at 09:02 UT. As a result of the intensified eastward flow of magnetopause current following an IP shock, a typical SI was triggered as indicated by the sudden enhancement of the SYM-H index. It can be seen that the vertical dashed line indicates SI onset. From the analysis of the SYM-H index variations, we found that the SI magnitude shifted from ∼8 to ∼35 nT (depicting a sudden rise of about 27 nT) following the IP shock. As the SYM-H reached its maximum at ∼10:01 UT, it dropped slightly, followed by a moderate decline, and remained steady at 27 nT during the period under consideration.

21699402, 2023, 3, Downloaded from https://agupubs.onlinelibrary.wiley.com/doi/10.1029/2022JA030565, Wiley Online Library on [11/07/2024]. See the Terms and Conditions (https://onlinelibrary.wiley.com/terms-and-conditions) on Wiley Online Library for rules of use; OA articles are governed by the applicable Creative Commons License

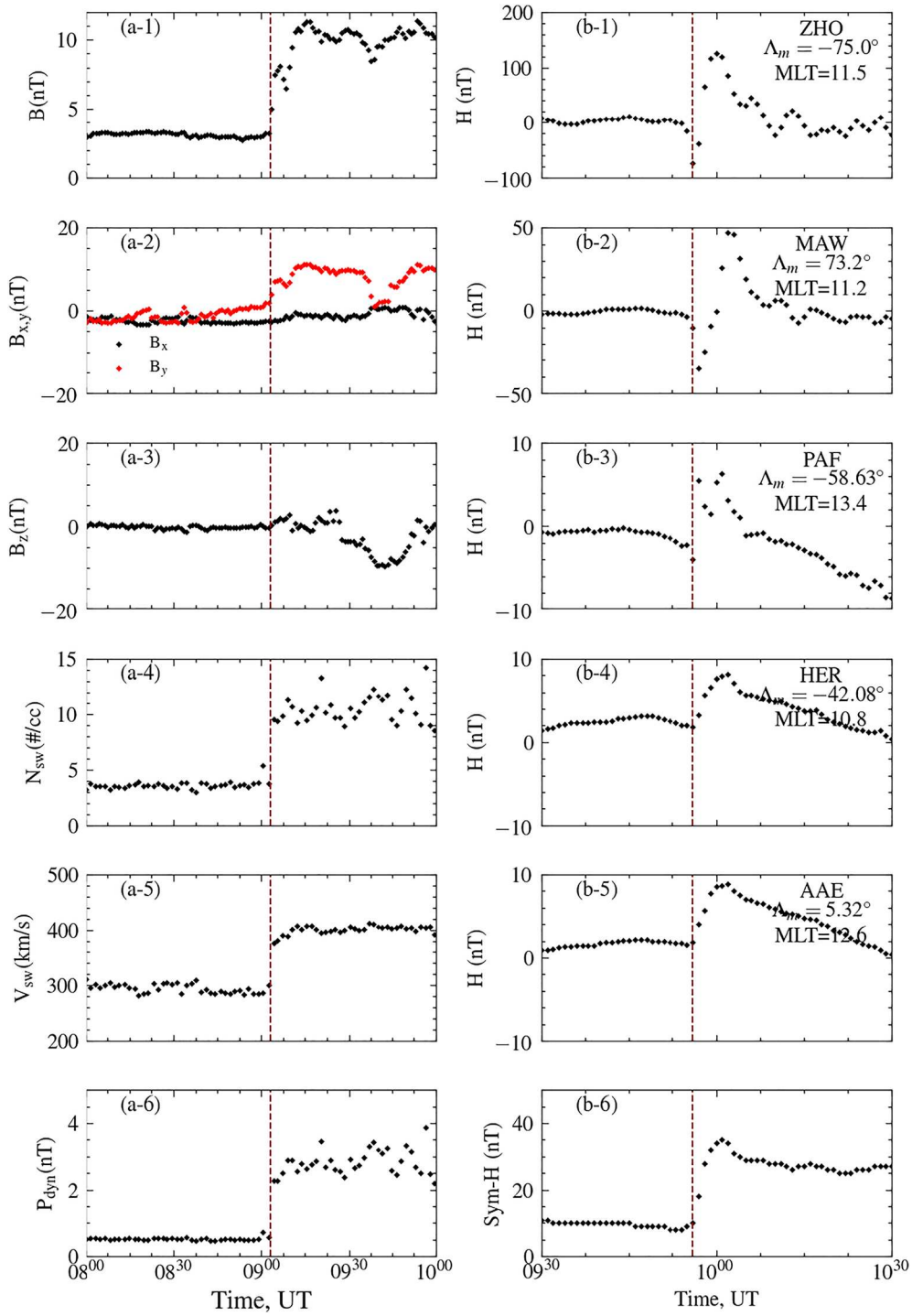

Figure 2. (a-1–6) IMF and solar wind plasma conditions between 08:00 and 10:00 UT on 16 June 2012. From top to bottom panels present IMF total B_t, B_x and B_y, B_z, number density N_{sw}, velocity V_{sw}, and dynamic pressure P_{dyn} in the GSM coordinate. (b-1–5) Geomagnetic field variations observed by ground-based magnetometers distributed from high latitude to low latitude [ZHO, Mawson (MAW), Port-aux Francias (PAF), Hermanus (HER), Addis Ababa (AAE)], and (b-6) Geomagnetic SYM-H index. The vertical dashed lines in panels (a) and (b) indicate the interplanetary shock and the sudden impulse onset, respectively.

21699402, 2023, 3, Downloaded from https://agupubs.onlinelibrary.wiley.com/doi/10.1029/2022JA030565, Wiley Online Library on [11/07/2024]. See the Terms and Conditions (https://onlinelibrary.wiley.com/terms-and-conditions) on Wiley Online Library for rules of use; OA articles are governed by the applicable Creative Commons License

21699402, 2023, 3, Downloaded from https://agupubs.onlinelibrary.wiley.com/doi/10.1029/2022JA030565, Wiley Online Library on [11/07/2024]. See the Terms and Conditions (https://onlinelibrary.wiley.com/terms-and-conditions) on Wiley Online Library for rules of use; OA articles are governed by the applicable Creative Commons License

As described above, the impact of the IP shock on Earth's space causes a global electromagnetic response in Earth's geomagnetic fields and plasma environment. Magnetometer observations presented in Figure 2b demonstrate the presence of geomagnetic perturbations in the horizontal components of the magnetic field following SI onset. The measurements of the geomagnetic field obtained from low latitude magnetometers in the southern hemisphere, such as the AAE and HER stations, show an apparent stepwise increase in the horizontal component. Observations made simultaneously by magnetometers located at high latitudes revealed rapid oscillations. PAF observations at the subauroral latitude demonstrate a positive pulse preceding SI onset, followed by a negative pulse. In contrast, observations made from magnetometers situated at auroral latitudes indicate complex fluctuations in the geomagnetic field. There was a slight decline in field strength measured at the two magnetometers (ZHO and MAW), followed by a sudden increase near the magnetic noon.

3.2. Cusp Ionosphere Vertical Motion and Associated Plasma Convection

In this subsection, we discuss the impact of IP shock on the polar ionosphere observed by ZHO digisonde and SuperDARN HF radars. In Figure 3, we depict the time evolution of the ionospheric vertical drifts, electron density profiles, and the evolution of the *E* layer ionization as observed by the ZHO digisonde. Figures 3a–3c present skymaps before, during, and after the IP shock reaches the geospace. Panels show Doppler frequency shifts, which depict plasma drift motions, observed using ZHO digisonde and color-coded by the color bar on the right. Specifically, blue and red represent motion toward (blueshift) and away (redshift) from the digisonde, respectively. Based on the zenith and azimuth look angle we extracted vertical (V_z) plasma drift velocity components in m/s. These estimates and associated uncertainties are provided in each panel. Figures 3d–3f present ionospheric electron density profiles in the form of an ionogram. The left, middle and right panels display the density profiles before, seconds after, and minutes after the IP shock arrival, respectively. The scaled parameters, namely, plasma frequency of the F1-layer (foF1), plasma frequency of the F2-layer (foF2), plasma frequency of the *E* layer, and height of the *E* layer are provided. These parameters are also labeled by vertical and horizontal lines in each panel. Figure 3g presents the time evolution of scaled parameters, namely, foE_s (in red) and $h'E_s$ (in blue), from the ionograms. The SI onset time is marked by the vertical black dashed line.

Following the impingement of the fast-forward IP shock, the vertical plasma drift velocity, presented in Figures 3a–3c, shows a rapid change in direction and magnitude. Before the IP shock arrival skymap shows (Figure 3a) a relatively quiet background with nearly zero average Doppler frequency shifts, representing a mean zero vertical velocity. Seconds after the shock arrival we see sudden enhancement in vertical Doppler motion reaching an average velocity of ∼246 m/s, depicting a sudden apparent downward movement of the ionosphere (Figure 3b). Figure 3c presents a depression in vertical Doppler motion reaching an average velocity of ∼−154 m/s, depicting a sudden apparent upward motion of the ionosphere that lasts less than 3-min (scan time of the Digisonde). However, Digisonde observed a mixture of upward and downward Doppler frequency shifts appearing in the off-zenith area in its field of view, suggesting a change in ionospheric propagation condition that is beyond the scope of this study. In conjunction, the ionograms presented in the middle row provide reasoning behind the sudden downward motion in response to the IP shock. Figure 3d presents the plasma density profile with auto-scaling parameters as follows: foF1 = 2.7 MHz and foF2 = 5.7 MHz. Figure 3e presents the density profile 2-min after the impingement that shows a presence of E_s-layer with foE_s = 3.8 MHz and a reduction in backscatter echoes. Figure 3f shows the density profile 5 min after the impingement, where we can see the persistent E_s-layer with foE_s = 3.8 MHz and the reappearance of backscatter echoes. Finally, the time-series plot presented in Figure 3g shows an existing E_s-layer around 130 km with an effective plasma frequency of 2.5 MHz, before the impingement. Following the IP shock, we see a strong E_s-layer with foE_s = 3.8 MHz at relatively lower altitudes ∼110 km.

IP shock drives magnetohydrodynamic waves that transform the magnetosphere into a new compressed steady-state configuration to balance with the increased solar wind pressure. A sudden change in the magnetic field geometry associated with SI results in perturbed VLF chorus wave activity, which could give rise to this enhanced energetic electron precipitation along the magnetic field lines (Gail et al., 1990; Zhou et al., 2015). To validate the HF absorption following the SI onset we present the number echoes from the SuperDARN ZHO radar and HF absorption observations from the Yellow River station in Svalbard, which is magnetically conjugate to the ZHO station, in Figure 4. The red vertical lines in panels represent the SI onset time (09:56 UT). We see a sudden dip in the number of backscatter echoes and a jump in riometer HF absorption following the SI onset.

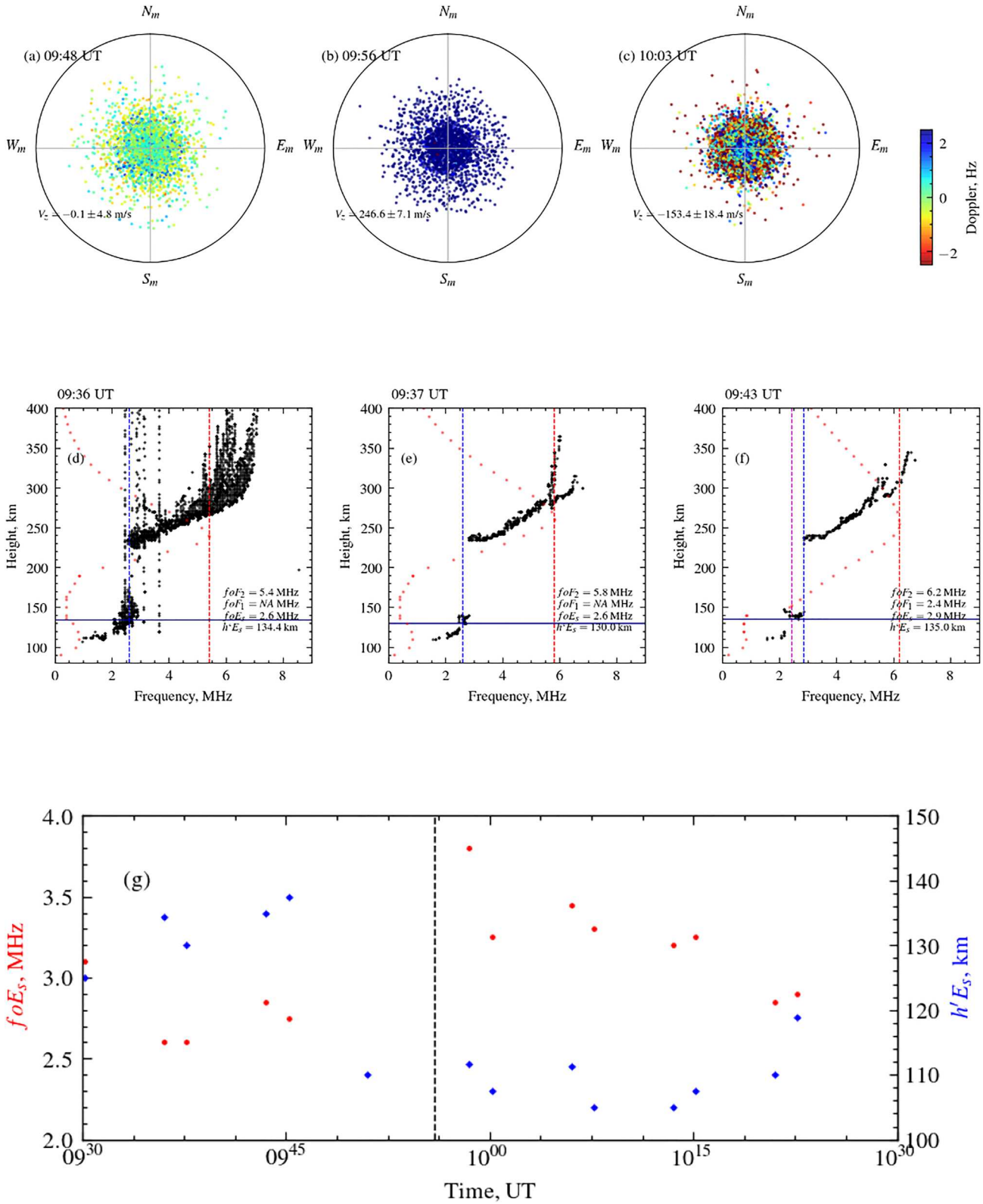

Figure 3.

21699402, 2023, 3, Downloaded from https://agupubs.onlinelibrary.wiley.com/doi/10.1029/2022JA030565, Wiley Online Library on [11/07/2024]. See the Terms and Conditions (https://onlinelibrary.wiley.com/terms-and-conditions) on Wiley Online Library for rules of use; OA articles are governed by the applicable Creative Commons License

21699402, 2023, 3, Downloaded from https://agupubs.onlinelibrary.wiley.com/doi/10.1029/2022JA030565, Wiley Online Library on [11/07/2024]. See the Terms and Conditions (https://onlinelibrary.wiley.com/terms-and-conditions) on Wiley Online Library for rules of use; OA articles are governed by the applicable Creative Commons License

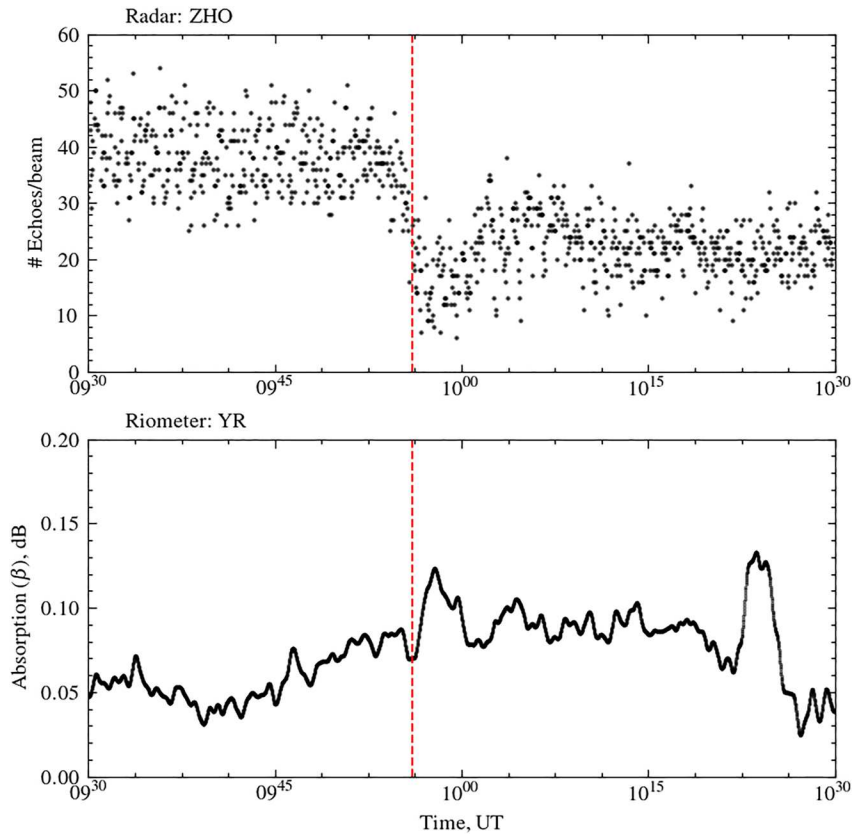

Figure 4. (a) Super Dual Auroral Radar Network backscatter echo counts from ZHO radar. (b) Ionospheric high-frequency absorption data was observed using Yellow River Riometer data located at Svalbard. Vertical red lines in panels (a) and (b) represent sudden impulse onset at 09:56 UT.

The observations suggest an enhancement in ionospheric HF absorption phenomena (Chakraborty et al., 2018; Chakraborty, 2021; Chakraborty, Bake, et al., 2021; Fiori et al., 2018) driven by energetic particle precipitation following the SI onset. We observe an early response in SuperDARN with respect to the riometer and show a delay before reaching a maximum drop in backscatter count. Primarily the delay can be attributed to ionospheric sluggishness, which is an inertial property of the ionosphere that manifests as a lag of the ionospheric response to a solar driver (Chapter 4 of Chakraborty, 2021). Previous studies have shown that as SuperDARN operates at much lower frequencies and traverses twice (four) times through the ionosphere, it is more sensitive to HF absorption than the riometer (Chakraborty et al., 2018; Fiori et al., 2018).

Ionospheric horizontal plasma motion (convection maps) was obtained from SuperDARN radar observations. As described above, we first present the observations from SuperDARN ZHO and MCM radars, which show the evolution of the LoS Doppler measurements throughout this IP shock passage by the magnetosphere. During the SI disturbance, ZHO radar has the advantage of monitoring longitudinal plasma flow around the convection throat region between 12 and 14 MLT (centered around 12 MLT) near the dayside cusp region at the convection boundary, while MCM radar provides the approximate latitudinal sunward and antisunward flow observational results. Figure 5 shows the range-time-intensity (RTI) plots of the LoS Doppler velocity from representative beams of these two radars mentioned in the upper-left of each panel. The LoS Doppler velocity in the panels of Figure 5 is

Figure 3. (a–c) Skymaps showing Doppler frequency shift associated with the vertical and horizontal plasma drift motion, observed by the ZHO digisonde at 09:48, 09:56, and 10:03 UT. Frequency shifts due to plasma drift motions toward or away from the digisonde are color-coded by blue or red, respectively. Mean vertical (V_z) Doppler velocities are provided in each panel with associated standard error. (d–f) Ionograms showing electron density profile at 09:52, 09:58, and 10:00 UT, overhead ZHO station. The scaled profile is also shown in each panel by red dotted markers. Scaled parameters, foF_2, foF_1, foE_s, and $h'E_s$ are marked by vertical red, magenta, blue, and horizontal dark blue lines, respectively, and their values are provided in each panel. (g) Variations of sporadic E layer's frequency (foE_s in red) and associated height ($h'E_s$ in blue) with respect to sudden impulse (SI) onset. The SI onset time (~9:56 UT) corresponds to the middle panels of the top two rows and is marked by the vertical black line in panel (g).

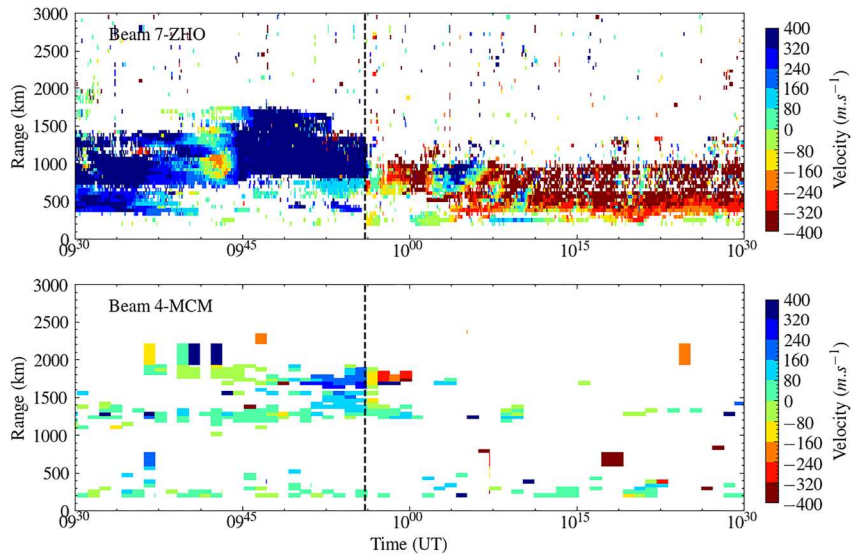

Figure 5. Super Dual Auroral Radar Network range-time-intensity plots showing line-of-sight Doppler velocity from beam 7 of ZHO and beam 4 of McMurdo radars. LoS Doppler velocities are color-coded according to the scales on the right. The vertical dashed lines represent the sudden impulse onset time.

color-coded by the color bar on the right, indicating the plasma flow toward (blueshift) and away (redshift) from the radar station, respectively.

We see a sudden change in LoS Doppler velocity magnitudes and directions in both radars. Before the IP shock arrival denoted by the vertical dashed line, ZHO radar observed a strong LoS plasma motion toward the ZHO station reaching over 800 m/s, suggesting a typical westward return flow toward the convection throat region near magnetic local noon (12 MLT). However, after the impingement induced by the fast forward IP shock, LoS Doppler velocity immediately switched its direction from westward to eastward. Note that this flow reversal lasts about ∼6 min, from 9:56 to 10:02 UT, following a ∼4 min of pre-reversal/pre-SI onset flow pattern. Finally, the convection flow became eastward and remained for the rest of the plot period. LoS ionospheric plasma flow velocity measured by the SuperDARN MCM radar also shows a similar flow reversal. Just after the SI onset, meridional plasma flow, specifically irregularities from far range gates, changes its direction from antisunward flow to sunward flow for a brief period. Observations from both radars, presented in Figure 5, suggest a flow reversal following the IP shock.

To get the large-scale ionospheric convection shape, Figure 6 displays three sequences of global-scale convection patterns in the southern hemisphere obtained using observations from 7 radars operating during the period under consideration. The convection flow direction of each panel, near the polar cusp ionospheric convection throat, is marked by black lines. Localized convection at 09:54 UT showed strong return flow in the early postnoon sector, which was denoted by reddish dots in the left panel. The convection pattern is consistent with the general twin convection cells pattern in dawn and dusk. During the initial compression state, as shown in the middle panel of Figure 6, the magnitude of plasma flow around the convection throat region reduced dramatically, as indicated by a few black dots with a flow speed of less than 200 m/s. Simultaneously, plasma flow in the central polar cap reversed from antisunward to sunward, forming localized counterclockwise convection cells. Large-scale ionospheric convection pattern recovered to two cells pattern with antisunward polar cap flow as shown in the right panel of Figure 6. We speculate this change observed in horizontal convection flow is driven by the change in the dawn-to-dusk electric field following the IP shock.

4. Discussion

This study examines the polar ionospheric transient responses to the IP shock on 16 June 2012. We analyzed the data from ground-based instruments. In our study, we observed a geomagnetic SI caused by the passage of the IP shock, which suggests that the IP shock signature observed on the dayside sector extends from the equator to

21699402, 2023, 3, Downloaded from https://agupubs.onlinelibrary.wiley.com/doi/10.1029/2022JA030565, Wiley Online Library on [11/07/2024]. See the Terms and Conditions (https://onlinelibrary.wiley.com/terms-and-conditions) on Wiley Online Library for rules of use; OA articles are governed by the applicable Creative Commons License

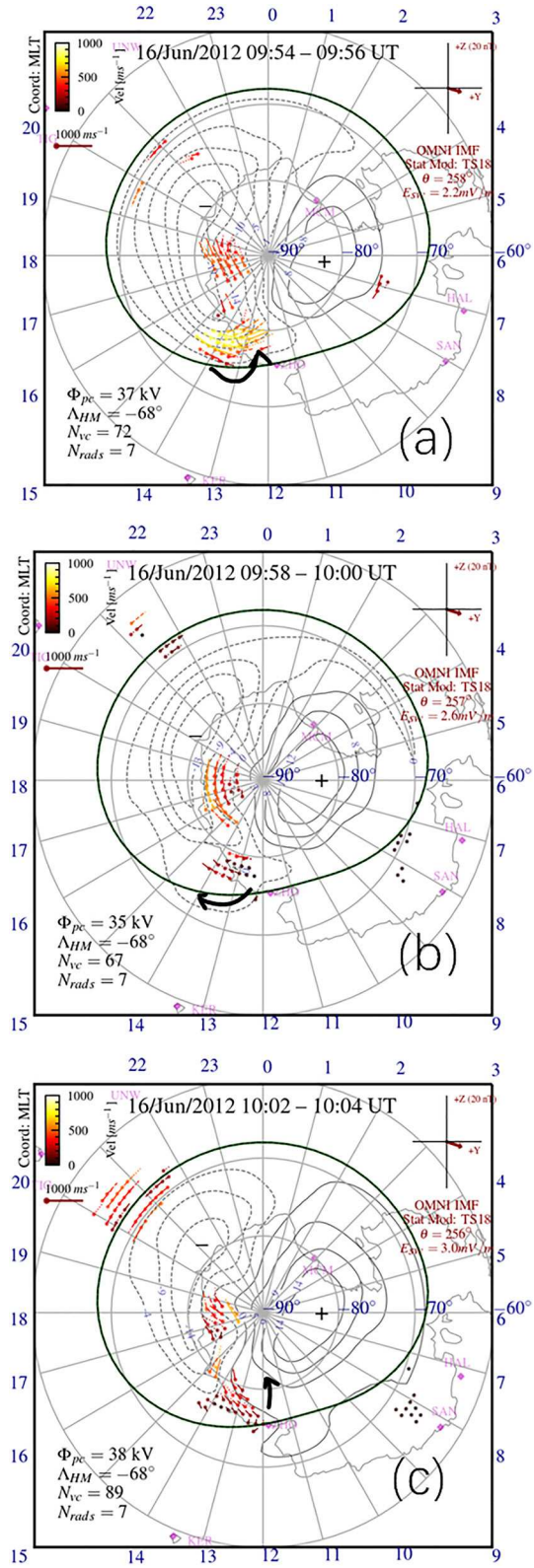

Figure 6.

21699402, 2023, 3, Downloaded from https://agupubs.onlinelibrary.wiley.com/doi/10.1029/2022JA030565, Wiley Online Library on [11/07/2024]. See the Terms and Conditions (https://onlinelibrary.wiley.com/terms-and-conditions) on Wiley Online Library for rules of use; OA articles are governed by the applicable Creative Commons License

21699402, 2023, 3, Downloaded from https://agupubs.onlinelibrary.wiley.com/doi/10.1029/2022JA030565, Wiley Online Library on [11/07/2024]. See the Terms and Conditions (https://onlinelibrary.wiley.com/terms-and-conditions) on Wiley Online Library for rules of use; OA articles are governed by the applicable Creative Commons License

southern high latitudes and in the geomagnetic SYM-H index. Observations indicate a thick *E* region ionization at an altitude of approximately 110 km with an apparent ionospheric downward motion. In addition, we found a sudden ionospheric convection reversal observed by the SuperDARN HF radars right after the SI onset.

Following an IP shock passage, a sudden compression of the magnetopause results in a change in the configuration of the magnetic field lines within the magnetosphere. The variations in the magnetic field following the arrival of the IP shock indicate that IP shock compression promotes more homogeneous background magnetic field configurations in the near-equatorial dayside magnetosphere. In a study by Zhou et al. (2015), it was found that the threshold of nonlinear whistler-mode chorus wave growth inside the magnetosphere is likely to be reduced following of the IP shock, which favor chorus wave generation. Due to the intensified wave-particle interaction, more energetic particles inside the loss cone along the magnetic field lines flow into the polar latitude ionosphere (*D*, *E*, and *F*-regions) following an IP shock (Fu et al., 2012; Liu et al., 2015; Shi et al., 2012; Zhou et al., 2003).

Previous research by MacDougall and Jayachandran (2005) has indicated that E_s occurrence is based on the convergence effects on ionization of electric fields. In addition, the study suggests that an existing Es layer can drop to ∼110 km from ∼130 km following a sudden change in the electric field. The study also suggests that vertical velocity can be attributed to the sudden change in the electric field. Following Kirkwood and Nilsson (2000), we understand the drift-convergence mechanism can create Es-layer. Motion of ions in the high and polar latitudes govern by the electric fields, natural winds, and ambipolar diffusion. In drift-convergence mechanism, the downward vertical ion motion following a sudden change electric field can form an Es layer around 110–130 km. In a study, Kirkwood and von Zahn (1991) found a weak layer at 125 km, which could be explained by E-field drift-convergence of molecular (NO^+, O_2^+) ions, and Kirkwood and von Zahn (1992), using the EISCAT (European Incoherent Scatter Scientific Association) Tromsø UHF (Ultra High Frequency) radar, reported a weak layer at 120 km which could be explained by a strong NW directed E-field gathering metallic ions.

A notable observational signature of this cusp ionosphere response to the IP shock impingement includes a brief downward horizontal plasma motion recorded by the digisonde at ZHO (see Figure 3). This motion lasted for about 3–6 min. To our knowledge, this type of high-latitude transient cusp ionosphere vertical motion is not been previously reported. According to Zong et al. (2010), the equatorial dayside ionosphere shows upward (downward) motion depending on the upstream component of the IMF turning southward (northward). The middle and high latitude ionospheres have seen an increase in TEC following an IP shock, which is thought to be associated with intensified energetic particle precipitation. The magnetosphere-ionosphere convection mechanism is controlled by both electric and magnetic fields (Tanaka, 2007). This vertical plasma motion identified in the HF spectrum may be due to two mechanisms: (a) an apparent downward movement of the ionosphere due to an increase in ionospheric density, and (or) (b) a change in ionospheric vertical motion related to a change in the magnetospheric electric field. Previous studies have found that HF radars do observe a sudden increase in downward vertical motion of the ionosphere which is primarily contributed by the change in the ionospheric refractive index following a sudden ionospheric density enhancement (Chakraborty et al., 2018, 2019; Chakraborty, Qian, et al., 2021; Fiori et al., 2018).

The SuperDARN ZHO radar measured plasma flow in early post noon was immediately reversed from strong westward to apparent eastward just after the SI onset, while central polar cap flow reversal from antisunward to sunward was also observed simultaneously by MCM. Both SuperDARN radar observations imply that a certain field aligned current (FAC) current formed instantly associated with the IP shock-driven sudden compression to the magnetosphere (Bristow & Lummerzheim, 2001). The SI model of Araki (1994) indicates that the FAC enters the polar ionosphere in the post noon sector during the PI stage. It is expected that a convection vortex induced by downward FAC should be observed in the post-noon sector. The dusk side polar ionospheric convection pattern is shown in Figure 6 as a large-scale clockwise cell before the arrival of the IP shock. In the immediate aftermath of the SI onset, a small convection cell formed in the post noon sector close to MLT-noon denoted by the dark black line, which is most likely initiated by a downward FAC that formed during the PI stage. A similar SI-related observation of plasma flow reversal with a counterclockwise convection vortex was reported previously (Liu

Figure 6. Super Dual Auroral Radar Network ionospheric convection patterns between 09:54 to 10:04 UT. Fitted map velocity vectors are also shown inside each panel and color-coded by the color bar on the left. The dot at the end of the vector represents the starting location of the velocity vector. Panels have a time cadence of 4-min. Estimated cross polar-cap potential (CPCP, Φ_{pc}), Heppner-Maynard boundary (Λ_{HM}), number of radar (N_{rads}), and gridded vectors used for convection mapping are provided in each panel. IMF condition for the 2-min window is presented in the top right corner. The thick black line near the 12-MLT convection boundary represents the direction of the effective velocity vector.

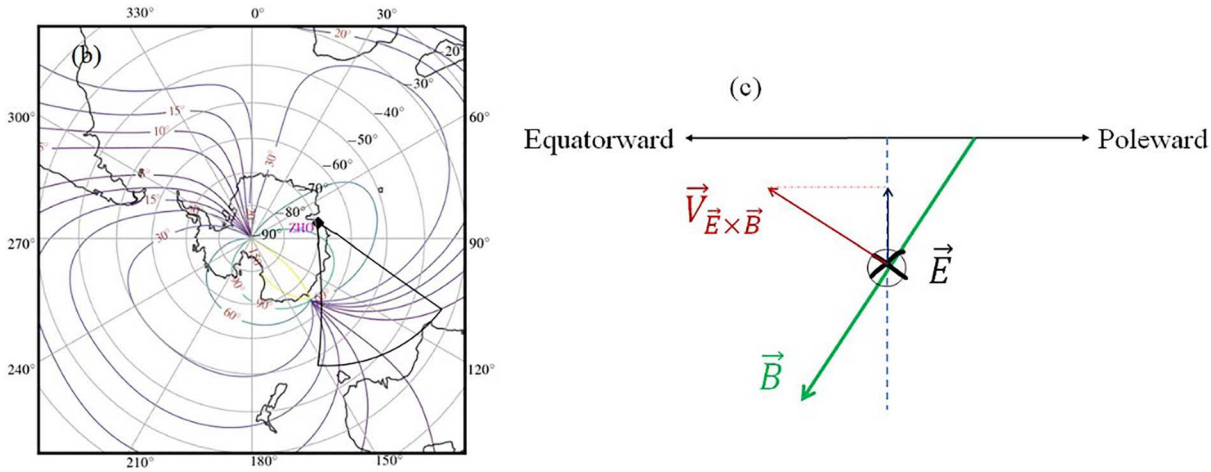

Figure 7. (a) Contour plots of magnetic inclination angle overlaid on FoV of the Super Dual Auroral Radar Network ZHO station, and (b) schematic illustration of the geometry for the downward motion associated with dusk-to-dawn electric field induced $\vec{E} \times \vec{B}$ drift in the meridional plane. Dusk-to-dawn electric field $\vec{E}$ was denoted by the circled cross sign.

et al., 2011). According to Liu et al. (2011), this change in convection flow is associated with a downward FAC that forms during the PI stage of the SI.

The ionospheric current for the PI is caused by a dusk-to-dawn electric field transmitted to the polar ionosphere from the compressional wavefront propagating in the dayside magnetosphere (Araki, 1994). As illustrated in Figure 7, the schematic diagram shows the geometry associated with induced plasma drift in the meridional plane looking from the dusk to dawn sector. The coordinates are shown as low and high latitudes marked by equatorward and poleward, respectively. The contour plot of the magnetic inclination angle suggests the steepness of magnetic field lines over the FoV of the SuperDARN ZHO radar. Note that most of the observations from ZHO radar being confined to less than 40 range gates which are associated with an average inclination angle $\geq 75°$ (refer to Figure 7). The schematic diagram for interpreting such dusk-to-dawn electric field-induced vertical downward motion shows the $\vec{E} \times \vec{B}$ drift perpendicular to the local magnetic field lines. Since the cusp magnetic field lines are somewhat oblique toward dayside, northward $\vec{E} \times \vec{B}$ drift shown as a red vector has the downward component along the vertical direction (short upward blue vector). Such a schematic illustration depicts - PI-induced prompt dusk-to-dawn electric field-driven downward plasma motion as observed by the digisonde at ZHO. This diagram explains the observational results shown in this event. We suggest that the transient vertical downward component due to the projection of the $\vec{E} \times \vec{B}$ drift is mainly responsible for decreasing the ionospheric irregularities to lower altitude and thus leading to the cusp ionosphere's brief downward motion. A modeling study is required to fully verify the physics behind the downward motion of the ionosphere and horizontal convection flow reversal observed by the SuperDARN radars.

5. Conclusions

As a geographical frontier toward the sun's direction, the polar cusp ionosphere is the first to react to the interaction between the solar wind and the magnetosphere. Thus, it is reasonable to anticipate that the polar cusp ionosphere will be significantly perturbed by the approaching IP disturbances. We study the transient response of the polar cusp ionosphere to external solar wind driving by examining the cusp ionospheric variations driven by an IP shock. We use observations from the Antarctic ZHO station and SuperDARN radars deployed in the southern hemisphere to analyze the effect and impact of the IP shock. Specifically, we found:

1. a brief vertical downward plasma motion and sudden appearance of a thick *E* region ionization around the noon MLT sector;
2. an increase in HF absorption observed by ZHO SuperDARN radar and riometer located at Yellow River, Svalbard station;
3. an associated horizontal convection reversal was also observed by ZHO and MCM SuperDARN radar and in the SuperDARN convection maps.

21699402, 2023, 3, Downloaded from https://agupubs.onlinelibrary.wiley.com/doi/10.1029/2022JA030565, Wiley Online Library on [11/07/2024]. See the Terms and Conditions (https://onlinelibrary.wiley.com/terms-and-conditions) on Wiley Online Library for rules of use; OA articles are governed by the applicable Creative Commons License

21699402, 2023, 3, Downloaded from https://agupubs.onlinelibrary.wiley.com/doi/10.1029/2022JA030565, Wiley Online Library on [11/07/2024]. See the Terms and Conditions (https://onlinelibrary.wiley.com/terms-and-conditions) on Wiley Online Library for rules of use; OA articles are governed by the applicable Creative Commons License

We also found the sudden appearance of the thick *E* region ionization and increase in ionospheric HF absorption are associated with the SI-driven electric field change, while the brief vertical drift in the ionosphere might be contributed by the change in the magnetospheric electric field. By examining the observations and comparing them with the SI model predictions of Araki (1994), we suggest that the rapid dusk-to-dawn electric field formed following the IP shock impingement plays a significant role in controlling cusp ionospheric transient dynamics.

The present study was conducted using data from the instruments deployed in the southern hemisphere. The conjugate phenomenon is expected to have implications in the northern hemisphere, which will require further examination and modeling.

Data Availability Statement

The SuperDARN radar data is from Virginia Tech (http://vt.superdarn.org/tiki-index.php). All other datasets and codes used in this study are linked on the GitHub page. We are grateful to SuperDARN PIs for sharing their data. SuperDARN is a collection of HF radars funded by national scientific funding agencies of Australia, Canada, China, France, Japan, Norway, South Africa, the United Kingdom, and the United States of America. Those lower latitude magnetometer data were obtained from INTERMAGNET (https://www.intermagnet.org/). The majority of analysis and visualization was completed with the help of free, open-source software tools such as matplotlib (Hunter, 2007), IPython (Perez & Granger, 2007), pandas (McKinney, 2010), and others (e.g., Millman & Aivazis, 2011). Our code and data are published in GitHub and Zenodo repositories (Chakraborty, 2022).

Acknowledgments
This work was supported by the National Scientific Foundation of China (Grants 41831072, 42130210, 42120104003, and 41974185), the National Key R&D Program of China (2021YFE0106400, 2022YFC2807205), the Shanghai Science and Technology Innovation Action Plan (21DZ1206100 and 22ZR1481200), the Chinese Meridian Project, and the MNR Innovative Youth Talents Program (12110600000018003921). Shibaji Chakraborty thanks to the National Science Foundation (NSF) and NASA for support under Grants AGS-1935110 and 80NSSC20K1380, respectively. National Arctic and Antarctic Data Center (http://www.chinare.org.cn) build upper atmospheric data sources. SC thanks the National Science Foundation for support under grant AGS-1935110. We acknowledge the NASA OMNI web for supplying IMF, solar wind, and geomagnetic parameters.

References

Araki, T. (1994). A physical model of the geomagnetic sudden commencement, in solar wind sources of magnetospheric ultra-low-frequency waves. *Geophysical Monograph Series*, *81*, 183–200.

Boudouridis, A., Lyons, L. R., Zesta, E., & Ruohoniemi, J. M. (2007). Dayside reconnection enhancement resulting from a solar wind dynamic pressure increase. *Journal of Geophysical Research: Space Physics*, *112*(A6). https://doi.org/10.1029/2006JA012141

Boudouridis, A., Lyons, L. R., Zesta, E., Ruohoniemi, J. M., & Lummerzheim, D. (2008). Nightside flow enhancement associated with solar wind dynamic pressure driven reconnection. *Journal of Geophysical Research: Space Physics*, *113*(A12). https://doi.org/10.1029/2008JA013489

Boudouridis, A., Zesta, E., Lyons, L. R., Anderson, P. C., & Lummerzheim, D. (2004). Magnetospheric reconnection driven by solar wind pressure fronts. *Annals of Geophysics*, *22*(4), 1367–1378. https://doi.org/10.5194/angeo-22-1367-2004

Bristow, W. A., & Lummerzheim, D. (2001). Determination of field-aligned currents using the Super Dual Auroral Radar Network and the UVI ultraviolet imager. *Journal of Geophysical Research: Space Physics*, *106*(A9), 18577–18587. https://doi.org/10.1029/2000JA000327

Bristow, W. A., Spaleta, J., & Parris, R. T. (2011). First observations of ionospheric irregularities and flows over the south geomagnetic pole from the Super Dual Auroral Radar Network (SuperDARN) HF radar at McMurdo Station, Antarctica. *Journal of Geophysical Research: Space Physics*, *116*(A12). https://doi.org/10.1029/2011ja016834

Chakraborty, S. (2021). *Characterization and modeling of solar flare effects in the ionosphere observed by HF instruments*. (PhD). Virginia Tech. Retrieved from http://hdl.handle.net/10919/103706

Chakraborty, S. (2022). shibaji7/IPShock_12jun2012: Submitted to JGR: Space physics for a revision (V1.0). *Zenodo*. https://doi.org/10.5281/zenodo.7039303

Chakraborty, S., Baker, J. B. H., Fiori, R. A. D., Ruohoniemi, J. M., & Zawdie, K. A. (2021). A modeling framework for estimating ionospheric HF absorption produced by solar flares. *Radio Science*, *56*(10), e2021RS007285. https://doi.org/10.1029/2021RS007285

Chakraborty, S., Baker, J. B. H., Ruohoniemi, J. M., Kunduri, B. S. R., Nishitani, N., & Shepherd, S. G. (2019). A study of SuperDARN response to co-occurring space weather phenomena. *Space Weather*, *17*(9), 1351–1363. https://doi.org/10.1029/2019SW002179

Chakraborty, S., Qian, L., Ruohoniemi, J. M., Baker, J. B. H., Mclnerney, J. M., & Nishitani, N. (2021). The role of flare-driven ionospheric electron density changes on the Doppler flash observed by SuperDARN HF radars. *Journal of Geophysical Research: Space Physics*, *126*(8), e2021JA029300. https://doi.org/10.1029/2021JA029300

Chakraborty, S., Ruohoniemi, J. M., Baker, J. B. H., & Nishitani, N. (2018). Characterization of short-wave fadeout seen in daytime SuperDARN ground scatter observations. *Radio Science*, *53*(4), 472–484. https://doi.org/10.1002/2017RS006488

Chen, X., Liu, J., Liu, R., Hu, H., Zhang, B., & Yukimatu, A. S. (2022). Comparison of Digisonde derived ion drifts and SuperDARN line-of-sight velocities over Zhongshan Station, Antarctica. *Polar Science*, *29*, 100789. https://doi.org/10.1016/j.polar.2022.100789

Chisham, G., Lester, M., Milan, S. E., Freeman, M. P., Bristow, W. A., Grocott, A., et al. (2007). A decade of the Super Dual Auroral Radar Network (SuperDARN): Scientific achievements, new techniques and future directions. *Surveys in Geophysics*, *28*(1), 33–109. https://doi.org/10.1007/s10712-007-9017-8

Fiori, R. A. D., Koustov, A. V., Chakraborty, S., Ruohoniemi, J. M., Danskin, D. W., Boteler, D. H., & Shepherd, S. G. (2018). Examining the potential of the Super Dual Auroral Radar Network for monitoring the space weather impact of solar X-ray flares. *Space Weather*, *16*(9), 1348–1362. https://doi.org/10.1029/2018SW001905

Fu, H. S., Cao, J. B., Mozer, F. S., Lu, H. Y., & Yang, B. (2012). Chorus intensification in response to interplanetary shock. *Journal of Geophysical Research: Space Physics*, *117*(A1). https://doi.org/10.1029/2011JA016913

Gail, W. B., Inan, U. S., Helliwell, R. A., Carpenter, D. L., Krishnaswamy, S., Rosenberg, T. J., & Lanzerotti, L. J. (1990). Characteristics of wave-particle interactions during sudden commencements: 1. Ground-Based observations. *Journal of Geophysical Research: Space Physics*, *95*(A1), 119–137. https://doi.org/10.1029/JA095iA01p00119

Greenwald, R. A., Baker, K. B., Dudeney, J. R., Pinnock, M., Jones, T. B., Thomas, E. C., et al. (1995). DARN/SuperDARN. *Space Science Reviews*, *71*(1), 761–796. https://doi.org/10.1007/BF00751350

Hu, H.-Q., Liu, E.-X., Liu, R.-Y., Yang, H.-G., & Zhang, B.-C. (2013). Statistical characteristics of ionospheric backscatter observed by SuperDARN Zhongshan radar in Antarctica. *Advances in Polar Science*, *24*(1), 13–31. https://doi.org/10.3724/sp.j.1085.2013.00019

Hunter, J. D. (2007). Matplotlib: A 2D graphics environment. *Computing in Science & Engineering*, *9*(3), 90–95. https://doi.org/10.1109/MCSE.2007.55

Ilie, R., Liemohn, M. W., Kozyra, J., & Borovsky, J. (2010). An investigation of the magnetosphere-ionosphere response to real and idealized co-rotating interaction region events through global magnetohydrodynamic simulations. *Proceedings of the Royal Society A: Mathematical, Physical and Engineering Sciences*, *466*(2123), 3279–3303. https://doi.org/10.1098/rspa.2010.0074

Jayachandran, P. T., Watson, C., Rae, I. J., MacDougall, J. W., Danskin, D. W., Chadwick, R., et al. (2011). High-latitude GPS TEC changes associated with a sudden magnetospheric compression. *Geophysical Research Letters*, *38*(23). https://doi.org/10.1029/2011gl050041

Jin, Y., Zhou, X., Moen, J. I., & Hairston, M. (2016). The auroral ionosphere TEC response to an interplanetary shock. *Geophysical Research Letters*, *43*(5), 1810–1818. https://doi.org/10.1002/2016GL067766

Kikuchi, T., Ohtani, A., & Isozaki, S. (1986). Ionospheric disturbances. Propagation disturbances of VLF radio waves on the trans-polar paths, in Solar-terrestrial disturbances of June-September 1982, edited. *Journal of the Radio Research Laboratory*, 203–217.

Kirkwood, S., & Nilsson, H. (2000). High-latitude sporadic-E and other thin layers—The role of magnetospheric electric fields. *Space Science Reviews*, *91*(3/4), 579–613. https://doi.org/10.1023/a:1005241931650

Kirkwood, S., & von Zahn, U. (1991). On the role of auroral electric fields in the formation of low-altitude sporadic-E and sudden sodium layers. *Journal of Atmospheric and Terrestrial Physics*, *53*(5), 389–407. https://doi.org/10.1016/0021-9169(91)90034-5

Kirkwood, S., & von Zahn, U. (1992). The role of magnetospheric electric fields in producing auroral zone thin layers. *Advances in Space Research*, *12*(10), 225–228. https://doi.org/10.1016/0273-1177(92)90471-9

Lepping, R. P., Acuna, M. H., Burlaga, L. F., Farrell, W. M., Slavin, J. A., Schatten, K. H., et al. (1995). The WIND magnetic field investigation. *Space Science Reviews*, *71*(1), 207–229. https://doi.org/10.1007/BF00751330

Lester, M., Chapman, P. J., Cowley, S. W. H., Crooks, S. J., Davies, J. A., Hamadyk, P., et al. (2004). Stereo CUTLASS—a new capability for the SuperDARN HF radars. *Annals of Geophysics*, *22*(2), 459–473. https://doi.org/10.5194/angeo-22-459-2004

Little, C. G., & Leinbach, H. (1959). The riometer-A device for the continuous measurement of ionospheric absorption. *Proceedings of the IRE*, *47*(2), 315–320. https://doi.org/10.1109/JRPROC.1959.287299

Liu, E.-X., Hu, H.-Q., Liu, R.-Y., Wu, Z.-S., Wu, M.-J., Yang, H.-G., & Zhang, B.-C. (2012). Diurnal variation of the HF radar echoes at Zhongshan Station and the influence of geomagnetic activity. *Chinese Journal of Geophysics*, *55*(9), 3066–3076. (in Chinese). https://doi.org/10.6038/j.issn.0001-5733.2012.09.024

Liu, J. J., Hu, H., Han, D., Yang, H., & Lester, M. (2015). Simultaneous ground-based optical and SuperDARN observations of the shock aurora at MLT noon. *Earth, Planets and Space*, *67*(1), 120. https://doi.org/10.1186/s40623-015-0291-2

Liu, J. J., Hu, H. Q., Han, D. S., Araki, T., Hu, Z. J., Zhang, Q. H., et al. (2011). Decrease of auroral intensity associated with reversal of plasma convection in response to an interplanetary shock as observed over Zhongshan station in Antarctica. *Journal of Geophysical Research: Space Physics*, *116*(A3), A03210. https://doi.org/10.1029/2010JA016156

Liu, R.-Y., Qian, S.-L., & He, L.-S. (1997). Preliminary experimental results about the digisonde portable sounder-4 at Zhongshan Station, Antarctica. *Progress in Geophysics*, *12*(4), 109–118. (in Chinese).

Liu, R.-Y., & Zhu, Y.-Q. (1999). Ionospheric drift properties and its response to the IMF conditions at Zhongshan Station, Antarctica. *Chinese Journal of Geophysics*, *42*(1), 30–40. (in Chinese).

MacDougall, J. W., & Jayachandran, P. T. (2005). Sporadic E at cusp latitudes. *Journal of Atmospheric and Solar-Terrestrial Physics*, *67*(15), 1419–1426. https://doi.org/10.1016/j.jastp.2005.07.011

McKinney, W. (2010). Data structures for statistical computing in Python. In S. van der Walt & J. Millman (Eds.), *Proceedings of the 9th Python in science conference* (pp. 56–61). https://doi.org/10.25080/Majora-92bf1922-012

Millman, K. J., & Aivazis, M. (2011). Python for scientists and engineers. *Computing in Science & Engineering*, *13*(2), 9–12. https://doi.org/10.1109/MCSE.2011.36

Nishitani, N., Ruohoniemi, J. M., Lester, M., Baker, J. B. H., Koustov, A. V., Shepherd, S. G., et al. (2019). Review of the accomplishments of mid-latitude Super Dual Auroral Radar Network (SuperDARN) HF radars. *Progress in Earth and Planetary Science*, *6*(1), 27. https://doi.org/10.1186/s40645-019-0270-5

Perez, F., & Granger, B. E. (2007). IPython: A system for interactive scientific computing. *Computing in Science & Engineering*, *9*(3), 21–29. https://doi.org/10.1109/MCSE.2007.53

Reinisch, B. W., Galkin, I. A., Khmyrov, G. M., Kozlov, A. V., Bibl, K., Lisysyan, I. A., et al. (2009). New Digisonde for research and monitoring applications. *Radio Science*, *44*(1). https://doi.org/10.1029/2008RS004115

Shi, R., Han, D., Ni, B., Hu, Z. J., Zhou, C., & Gu, X. (2012). Intensification of dayside diffuse auroral precipitation: Contribution of dayside Whistler-mode chorus waves in realistic magnetic fields. *Annals of Geophysics*, *30*(9), 1297–1307. https://doi.org/10.5194/angeo-30-1297-2012

Slinker, S. P., Fedder, J. A., Hughes, W. J., & Lyon, J. G. (1999). Response of the ionosphere to a density pulse in the solar wind: Simulation of traveling convection vortices. *Geophysical Research Letters*, *26*(23), 3549–3552. https://doi.org/10.1029/1999gl010688

Tanaka, T. (2007). Magnetosphere–ionosphere convection as a compound system. *Space Science Reviews*, *133*(1), 1–72. https://doi.org/10.1007/s11214-007-9168-4

Tsurutani, B., Mannucci, A., Iijima, B., Abdu, M. A., Sobral, J. H. A., Gonzalez, W., et al. (2004). Global dayside ionospheric uplift and enhancement associated with interplanetary electric fields. *Journal of Geophysical Research: Space Physics*, *109*(A8), A08302. https://doi.org/10.1029/2003ja010342

Yue, C., Zong, Q. G., Zhang, H., Wang, Y. F., Yuan, C. J., Pu, Z. Y., et al. (2010). Geomagnetic activity triggered by interplanetary shocks. *Journal of Geophysical Research: Space Physics*, *115*(A5), A00I05. https://doi.org/10.1029/2010ja015356

Zhou, C., Li, W., Thorne, R. M., Bortnik, J., Ma, Q., An, X., et al. (2015). Excitation of dayside chorus waves due to magnetic field line compression in response to interplanetary shocks. *Journal of Geophysical Research: Space Physics*, *120*(10), 8327–8338. https://doi.org/10.1002/2015JA021530

Zhou, X.-Y., Strangeway, R. J., Anderson, P. C., Sibeck, D. G., Tsurutani, B. T., Haerendel, G., et al. (2003). Shock aurora: FAST and DMSP observations. *Journal of Geophysical Research: Space Physics*, *108*(A4), 8019. https://doi.org/10.1029/2002JA009701

Zong, Q. G., Reinisch, B. W., Song, P., Wei, Y., & Galkin, I. A. (2010). Dayside ionospheric response to the intense interplanetary shocks–solar wind discontinuities: Observations from the digisonde global ionospheric radio observatory. *Journal of Geophysical Research: Space Physics*, *115*(A6), A06304. https://doi.org/10.1029/2009JA014796

21699402, 2023, 3, Downloaded from https://agupubs.onlinelibrary.wiley.com/doi/10.1029/2022JA030565, Wiley Online Library on [11/07/2024]. See the Terms and Conditions (https://onlinelibrary.wiley.com/terms-and-conditions) on Wiley Online Library for rules of use; OA articles are governed by the applicable Creative Commons License